The Astrophysical Journal, 985:88 (7pp), 2025 May 20 https://doi.org/10.3847/1538-4357/adcc17
© 2025. The Author(s). Published by the American Astronomical Society.
OPEN ACCESS

Comparing Observed Properties of Winds in Low-luminosity Active Galactic Nuclei with Theoretical Predictions

Fangzheng Shi (施方正)[1], Feng Yuan[2], Francesco Tombesi[3,4,5], and Fu-guo Xie[1]
[1] Shanghai Astronomical Observatory, Chinese Academy of Sciences, Shanghai, People's Republic of China; fzshi@shao.ac.cn
[2] Center for Astronomy and Astrophysics and Department of Physics, Fudan University, Shanghai 200438, People's Republic of China; fyuan@fudan.edu.cn
[3] Physics Department, Tor Vergata University of Rome, Via della Ricerca Scientifica 1, 00133 Rome, Italy
[4] INAF—Astronomical Observatory of Rome, Via Frascati 33, 00040 Monte Porzio Catone, Italy
[5] INFN—Rome Tor Vergata, Via della Ricerca Scientifica 1, 00133 Rome, Italy
Received 2025 February 11; revised 2025 April 9; accepted 2025 April 12; published 2025 May 15

Abstract

Theoretical and numerical simulations of black hole hot accretion flows have shown the ubiquitous existence of winds and predicted their properties, such as velocity and mass flux. In this paper, we have summarized from the literature the physical properties of winds launched from low-luminosity active galactic nuclei (LLAGN), which are believed to be powered by hot accretion flows, and compared them with theoretical predictions. We infer that for both ultrafast outflows and hot winds, the observed wind velocity as a function of their launching radius and the ratio between wind mass flux and black hole accretion rate show good consistency with theoretical predictions. For the prototype LLAGN M81* with abundant observational data, we have examined various observed properties of wind in detail, including velocity, mass flux of the wind, the power-law index of the radial profile of inflow rate, and the jet-to-wind power ratio. Good agreements are found with theoretical predictions, providing strong support to the theory of wind launched from hot accretion flows.

Unified Astronomy Thesaurus concepts: Low-luminosity active galactic nuclei (2033); Supermassive black holes (1663); Accretion (14)

1. Introduction

Black hole accretion can be divided into cold mode and hot mode according to the mass accretion rate. The cold-mode accretion includes standard thin disks and super-Eddington accretion (N. I. Shakura & R. A. Sunyaev 1973; M. A. Abramowicz et al. 1988). It usually happens in a black hole with a high or intermediate accretion rate, like in bright quasars and Seyfert galaxies. However, we focus on hot-mode accretion where the Eddington ratio (between active galactic nucleus, AGN, bolometric luminosity and the Eddington limit) falls below the threshold of 2% (F. Yuan & R. Narayan 2014). Such black holes with low accretion rate would manifest themselves as low-luminosity active galactic nuclei (LLAGN). The majority of the local galaxies are in low-luminosity and quiescent states (L. C. Ho 2008). As an analog of the black hole binary in a low–hard state, LLAGN are found to have a similar accretion structure. As the accretion rate of black hole drops, the inner accretion thin disk would be truncated and replaced by a geometrically thick, optically thin, radiatively inefficient hot accretion flow (F. Yuan & R. Narayan 2014; R. Narayan & I. Yi 1994, 1995; A. A. Esin et al. 1997).

Both theory study and MHD numerical simulations of black hole accretion in the past decade have predicted the existence of strong wind launched from hot accretion flows (R. D. Blandford & M. C. Begelman 1999; F. Yuan et al. 2012a, 2012b; R. Narayan et al. 2012; F. Yuan et al. 2015; D.-F. Bu et al. 2016). The detailed properties of the hot wind (HW), such as the velocity, mass flux, and special distribution, have been investigated based on three-dimensional general relativistic MHD (GRMHD) simulations (F. Yuan et al. 2015; H. Yang et al. 2021). HW not only affects the dynamics of accretion inflow around the black hole but also serves as an important medium in AGN feedback (A. C. Fabian 2012; J. Kormendy & L. C. Ho 2013; R. Weinberger et al. 2017; F. Yuan et al. 2018; D. Yoon et al. 2019). By including the HW feedback in the numerical simulation study of the evolution of an individual elliptical galaxy, it has been shown that wind plays an important role in controlling the luminosity of the black hole and its growth (D. Yoon et al. 2019).

Observational detection of wind driven by hot accretion flow, however, has remained scarce and indirect for a long time. Q. D. Wang et al. (2013) reported a flat rather than increasing density profile of hot accretion flow around Sgr A* from high-resolution X-ray spectroscopy, implying indirectly that the existence of potential outflow suppresses the inflow. E. Cheung et al. (2016) inferred the presence of centrally driven, galactic-scale wind in a sample of typical quiescent galaxies hosting low-luminosity AGN around $z \sim 0.02$. The first direct observational evidence of HW driven by hot accretion flow in LLAGN has been detected through blue-shifted highly ionized iron emission lines in M81* and NGC 7213. The kinetic energy carried by these LLAGN winds can account for 10%–15% of total AGN bolometric luminosity (F. Shi et al. 2021, 2022). This is larger than the theoretical prediction that the mechanical efficiency generated by the hot accretion flows can hardly exceed 3% of the accretion mass energy flux claimed by A. Sądowski & M. Gaspari (2017). The observational evidence for the interaction between wind and the circumnuclear gas within the parsec scale has been found and is likely the physical mechanism of keeping the central AGN dim (F. Shi et al. 2024).

Ionized winds characterized by blueshifted absorption lines in X-ray or UV bands are ubiquitous in up to 30%–50% of

Original content from this work may be used under the terms of the Creative Commons Attribution 4.0 licence. Any further distribution of this work must maintain attribution to the author(s) and the title of the work, journal citation and DOI.

local (bright) AGN (D. M. Crenshaw & S. B. Kraemer 2012). Some ultrafast outflows (UFOs) could reach $\sim 10^4\,\mathrm{km\,s^{-1}}$, while most warm absorbers (WA) have a velocity ranging from $\sim 10^2$ to $\sim 10^3\,\mathrm{km\,s^{-1}}$. Many statistical studies have been carried on the whole sample or certain types of outflows in AGN (S. Laha et al. 2014, 2016; F. Fiore et al. 2017; M. Mehdipour & E. Costantini 2019). By comparing UFOs in both radio-loud and radio-quiet AGN, S. Mestici et al. (2024) suggest that these accretion disk winds could likely be produced by the same physical mechanism. More and more evidence supports that the launching mechanism of the black hole winds (specifically for UFOs) would be dominated by magnetically driven in the inner region of accretion flow (e.g., F. Yuan et al. 2015; H. Yang et al. 2021; K. Fukumura et al. 2022; W. Wang et al. 2022), and wind properties would depend on the accretion rate, black hole spin, and magnetic field configuration and strength (F. Yuan et al. 2015; H. Yang et al. 2021). The Eddington ratio of AGN hosting either UFO or WA spans a very wide range. Some of these AGN have an Eddington ratio below the threshold of 2%, where hot-mode accretion should dominate their inner accretion region according to the theory of black hole accretion (F. Yuan & R. Narayan 2014). However, systematic study of such winds detected in low-luminosity AGN remains scarce so far.

The aim of this work is to statistically summarize the common properties of outflows detected in LLAGN so far and to compare the results with the theory of wind launching in hot accretion flows. In Section 2, we first review the theoretical prediction of wind launched from hot accretion flows, then select a sample of outflows detected in the low-luminosity AGN with an Eddington ratio lower than the critical value $R_{\rm Edd} \lesssim 0.02$. Statistical results of winds in these LLAGN have been reported in Section 3. In Section 4, we analyze the observed wind velocity, mass flux of wind, and inflow of M81* in detail and compare them with the state-of-the-art theory of hot accretion flow wind. We summarize and discuss our results in Section 5.

2. Method

2.1. Physics of Hot Accretion Flow

In LLAGNs, the accretion flow consists of an outer truncated thin disk plus an inner hot accretion flow (T. Storchi-Bergmann et al. 1997; F. Yuan & R. Narayan 2004; R. S. Nemmen et al. 2014; A. J. Young et al. 2018). The truncation radius ($r_{\rm tr}$) is inversely correlated with the Eddington ratio (or the accretion rate; F. Yuan & R. Narayan 2014). In the present paper we focus on the wind launched from the inner hot accretion flow. While the existence of such a wind has been shown by some previous works (e.g., R. Narayan et al. 2012; F. Yuan et al. 2012a), they did not investigate its physical properties. Since the accretion flow is highly turbulent, to understand the wind properties, it is crucial to separate the real wind from the turbulent outflow. In literature, a widely adopted approach is to calculate a time average of the simulation data to filter out turbulence. However, since the wind is instantaneously produced, in this case, the real wind may also be filtered out.

To overcome this difficulty, F. Yuan et al. (2015) adopted a new "virtual test particle trajectory" approach. Different from the widely adopted time-averaged streamline approach, obtaining Lagrangian trajectories can adequately reflect the motion of fluid elements and thus discriminate between wind and turbulence. Using this approach, based on three-dimensional GRMHD numerical simulation data of black hole accretion, F. Yuan et al. (2015) successfully obtained the properties of the wind launched from a hot accretion flow. This work only deals with the standard and normal evolution (SANE) around a nonspinning black hole (SANE00). Later, H. Yang et al. (2021) extended this work to cases of both SANE and magnetically arrested disks (MADs) around black holes with various spin values (i.e., SANE98, MAD00, and MAD98). Here the number denotes the spin value of the black hole. For example, "98" denotes $a = 0.98$.

The net mass accretion rate in the hot accretion flow would decrease with the decreasing of radius as a result of the presence of the HW. The radial profile of the mass flux of the inflow $\dot{M}_{\rm in}$ can be well described as

$$\dot{M}_{\rm in}(r) = \dot{M}_{\rm in}(r_{\rm out})\left(\frac{r}{r_{\rm out}}\right)^{s}. \quad (1)$$

Here $r_{\rm out}$ denotes the outer boundary of the hot accretion flow. The values of s-index are (F. Yuan et al. 2015; H. Yang et al. 2021) as follows:

1. s = 0.54 for SANE00;
2. s = 0.91 for SANE98;
3. s = 0.18 for MAD00;
4. s = 0.42 for MAD98.

For a wind launched from a hot accretion flow, the wind velocities are predicted to be

$$v_{\rm wind} = 0.21 v_{\rm k}(r_{\rm tr}) \quad \text{(SANE00)}, \quad (2)$$

$$v_{\rm wind} = 0.66 v_{\rm k}(r_{\rm tr}) \quad \text{(SANE98)}, \quad (3)$$

$$v_{\rm wind} = 0.24 v_{\rm k}(r_{\rm tr}) \quad \text{(MAD00)}, \quad (4)$$

$$v_{\rm wind} = 0.64 v_{\rm k}(r_{\rm tr}) \quad \text{(MAD98)}. \quad (5)$$

Here $v_{\rm k}(r)$ refers to the Keplerian velocity at radius r (F. Yuan et al. 2015).

The mass flux of the wind increases with radius and would be comparable with the inflow rate at the outer boundary of the hot accretion flow (i.e., truncation radius $r_{\rm tr}$) $\dot{M}_{\rm out} \simeq \dot{M}_{\rm in,net}(r_{\rm tr})$. Thus the wind could efficiently suppress the mass inflow, making the net accretion rate at the black hole event horizon much smaller than the inflow rate at $r_{\rm tr}$ ($\dot{M}_{\rm in,net}(r_{\rm EH}) \ll \dot{M}_{\rm in,net}(r_{\rm tr})$).

2.2. Sample Selection

We retrieve the properties of all types of winds reported in low-luminosity AGN with X-ray observations from the literature, as summarized in Table 1. To obtain a reasonable sample size, we extend the Eddington ratio threshold to $R_{\rm Edd} \lesssim 0.04$ for AGN with a low-luminosity end.

For sources with multiple wind components reported, we select the component with the largest velocity to trace the wind as close to the central black hole as possible. This is because we are mainly interested in the wind launched from the accretion flow, while the closest component would be less subject to the interaction with the circumnuclear medium and represent the intrinsic wind properties. We take the average of parameters for wind components with the largest velocity reported in multiple literature with the same observations, while we keep as an independent record that derived from different observations. A total of 21 wind components discovered in 14 sources have

Table 1
Properties of Wind in the Low-luminosity AGN Sample

Source	Type	$M_{\rm BH}$ ($10^7\ M_\odot$)	$\log(R_{\rm Edd})$	$v_{\rm wind}$ (km s^{-1})	$\log(R_{\rm max})$ ($r_{\rm g}$)	$\log(r_{\rm tr,SANE00})$ ($r_{\rm g}$)	$\log(r_{\rm tr,MAD98})$ ($r_{\rm g}$)	$\dot{M}_{\rm in}$ ($M_\odot$ yr^{-1})	$\dot{M}_{\rm out}$ (min/max) ($M_\odot$ yr^{-1})
(1)	(2)	(3)	(4)	(5)	(6)	(7)	(8)	(9)	(10)
M81*	HW	7^{+2}_{-1}	$-4.64^{+0.07}_{-0.11}$	-2800^{+200}_{-200}	$3.7^{+0.3}_{-0.2}$	$2.69^{+0.15}_{-0.15}$	$3.66^{+0.15}_{-0.15}$	0.00008	$-/0.002$
NGC 7213	HW	8^{+16}_{-6}	$-3.0^{+0.8}_{-0.6}$	-1200^{+100}_{-200}	$3.9^{+0.4}_{-0.4}$	$3.3^{+0.6}_{-0.6}$	$4.3^{+0.6}_{-0.6}$	0.003	$-/0.08$
IRAS 050278	WA	$7.2^{+0.7*}_{-0.7}$	$-1.61^{+0.05}_{-0.04}$	-900^{+600}_{-30}	$10.1^{+0.2}_{-0.2}$	$3.68^{+0.07}_{-0.07}$	$4.65^{+0.07}_{-0.07}$	0.049	0.017/1952
NGC 3227	WA	$2.0^{+1.0}_{-0.4}$	$-1.73^{+0.10}_{-0.18}$	-1270^{+20}_{-120}	$3.85^{+0.05}_{-0.05}$	$3.4^{+0.2}_{-0.2}$	$4.3^{+0.2}_{-0.2}$	0.01	0.0016/0.0037
⋯	WA	⋯	⋯	-2060^{+240}_{-170}	$5.3^{+0.3}_{-0.3}$	$2.9^{+0.2}_{-0.2}$	$3.9^{+0.2}_{-0.2}$	⋯	0.0126/0.032
NGC 5548	WA	$9.3^{+0.6}_{-0.6}$	$-2.6^{+0.3}_{-1.1}$	3610^{+180}_{-270}	$6.75^{+0.12}_{-0.12}$	$2.47^{+0.07}_{-0.07}$	$3.44^{+0.07}_{-0.07}$	0.007	0.0155/9.35
⋯	WA	⋯	⋯	-1040^{+150}_{-150}	$6.32^{+0.18}_{-0.17}$	$3.56^{+0.11}_{-0.11}$	$4.53^{+0.11}_{-0.11}$	⋯	0.29/0.96
⋯	WA	⋯	⋯	-1180^{+150}_{-150}	$7.6^{+0.1}_{-0.1}$	$3.45^{+0.10}_{-0.10}$	$4.42^{+0.10}_{-0.10}$	⋯	0.05/3.95
3C59	WA	79^{+8*}_{-8}	$-1.41^{+0.05}_{-0.04}$	-3530^{+130}_{-130}	$7.85^{+0.05}_{-0.06}$	$2.49^{+0.07}_{-0.07}$	$3.46^{+0.07}_{-0.07}$	0.85	0.072/716
⋯	WA	⋯	⋯	-1000^{+120}_{-120}	$6.32^{+0.05}_{-0.06}$	$3.59^{+0.10}_{-0.11}$	$4.56^{+0.10}_{-0.11}$	⋯	0.51/12.1
3C382	WA	115^{+12*}_{-12}	$-1.55^{+0.05}_{-0.04}$	-1530^{+370}_{-370}	$7.21^{+0.12}_{-0.17}$	$3.22^{+0.17}_{-0.16}$	$4.19^{+0.17}_{-0.16}$	0.88	0.041/18
4C+74.26	WA	417^{+42*}_{-42}	$-1.70^{+0.05}_{-0.04}$	-1490^{+90}_{-90}	$7.10^{+0.05}_{-0.06}$	$3.24^{+0.08}_{-0.08}$	$4.21^{+0.08}_{-0.08}$	2.3	0.80/254
⋯	WA	⋯	⋯	-3000^{+500}_{-500}	$6.06^{+0.06}_{-0.07}$	$2.64^{+0.13}_{-0.13}$	$3.60^{+0.13}_{-0.13}$	⋯	0.75/88
Mrk 6	WA	$12.7^{+1.1}_{-1.1}$	$-1.84^{+0.04}_{-0.04}$	-4000^{+500}_{-500}	$6.69^{+0.06}_{-0.07}$	$2.39^{+0.11}_{-0.10}$	$3.36^{+0.11}_{-0.10}$	0.05	0.041/25.8
PKS 2135-14	WA	450^{+45*}_{-45}	$-1.74^{+0.05}_{-0.04}$	-1240^{+530}_{-530}	$7.4^{+0.2}_{-0.4}$	$3.4^{+0.3}_{-0.3}$	$4.4^{+0.3}_{-0.3}$	2.2	0.14/64
NGC 4151	WA	$2.37^{+0.17}_{-0.15}$	$-1.64^{+0.03}_{-0.03}$	-490^{+50}_{-50}	$4.3^{+0.2}_{-0.3}$	$4.21^{+0.08}_{-0.08}$	$5.18^{+0.08}_{-0.08}$	0.015	1.16/5.6
⋯	WA	⋯	⋯	-370^{+40}_{-40}	$5.69^{+0.19}_{-0.19}$	$4.46^{+0.08}_{-0.09}$	$5.43^{+0.08}_{-0.09}$	⋯	1.26/0.93
⋯	UFO	⋯	⋯	-31800^{+2100}_{-2100}	< 3.25	$0.59^{+0.07}_{-0.07}$	$1.55^{+0.07}_{-0.07}$	⋯	0.003/0.04
Mrk 205	UFO	40^{+358}_{-36}	$-1.9^{+1.0}_{-1.0}$	-30000^{+1200}_{-1200}	< 2.42	$0.2^{+1.1}_{-1.1}$	$1.1^{+1.1}_{-1.0}$	0.13	0.63/0.63
Cygnus A	UFO	250 ± 70	$-1.90^{+0.14}_{-0.11}$	-19000^{+10000}_{-7000}	< 3.34	$1.0^{+0.3}_{-0.3}$	$2.0^{+0.3}_{-0.3}$	0.9	7.7/247
NGC 7582	UFO	1.3 ± 0.3	-1.9 ± 0.1	-85000^{+900}_{-900}	<2.78	⋯	$0.69^{+0.15}_{-0.15}$	0.004	0.023/11.7

Note. (1) Source name; (2) outflow type: "HW" for hot wind, "WA" for warm absorbers, and "UFO" for ultrafast outflow; (3) black hole mass. Errors are determined by 10% uncertainties if no explicit error bars are provided in the literature for measurements marked by "*"; (4) Eddington ratio; (5) wind velocity; (6) location of wind assuming its depth equals its distance to the SMBH ($\Delta r = r$); (7)–(8) putative truncation radius assuming SANE- or MAD-type accretion flow surrounding the SMBH with spin a of 0 or 0.98; (9) mass inflow rate deduced from $L_{\rm bol}$; (10) lower/upper limit of the mass outflow rate.

been retrieved. Properties of these winds are collected from F. Shi et al. (2021, 2022), S. Laha et al. (2014, 2016), A. Markowitz et al. (2009), M. Mehdipour et al. (2021), Y. Wang et al. (2022), K. C. Steenbrugge et al. (2005), B. McKernan et al. (2007), M. Andrade-Velázquez et al. (2010), M. Mehdipour & E. Costantini (2019), S. B. Kraemer et al. (2005), F. Tombesi et al. (2010, 2011,2013), C. S. Reynolds et al. (2015), and S. Mestici et al. (2024), and black hole mass are taken from M. C. Bentz & S. Katz (2015).

We divide the collected wind components detected in the low-luminosity AGN into three categories. UFOs are characterized by blueshifted absorption lines with large bulk velocity higher than $\gtrsim 10^4$ km s^{-1} (F. Tombesi et al. 2010; G. A. Matzeu et al. 2023). HWs driven by hot accretion flow with large opening angle have first been detected in M81* and NGC 7213, traced by highly collisionally ionized iron emission lines with a blue-/redshift velocity of $\sim 10^3$ km s^{-1} in the hard X-ray band. Although the confirmed cases of HW remain scarce, growing evidence indicates their prevalence in LLAGN. WAs are mass outflows of ionized clouds characterized by blueshifted absorption lines in soft X-ray of UV bands with typical velocity ranging $\sim 10^2$ km s^{-1}-$\sim 10^3$ km s^{-1}.

Assuming the observed wind originates from the outer edge ($r \simeq r_{\rm tr}$) of the hot accretion flow, the velocity of winds would remain almost constant as the wind freely propagates outward and before it encounters the interstellar medium (ISM; C. Cui & F. Yuan 2020). We consider two extreme assumptions: SANE00 and MAD98. Based on Equations (2) and (5), we deduce the putative truncation radius $r_{\rm tr}$ from the observed velocity of wind $v_{\rm wind}$, as recorded in Table 1. We neglect the projection effect caused by the viewing angle for simplicity.

We use $R_{\rm max}$ to describe the average location of wind determined through observation (either emission or absorption). For HW detected with emission lines, $R_{\rm max}$ represents the radius where 50% of the total luminosity of the blueshifted Fe XXVI line resides within (from Figure 2 in F. Shi et al. 2024). For WA and UFO, by combining the column density $N_{\rm H} = n_{\rm H} V_{\rm f} \Delta r$ and ionization parameter $\xi = \frac{L_{\rm ion}}{n_{\rm e} r^2}$ derived from spectral modeling in the literature, while assuming the depth of wind is roughly equivalent to its distance to black hole $\Delta r \simeq r$, the wind location is determined by $R_{\rm max} = \frac{L_{\rm ion} V_{\rm f}}{\xi N_{\rm H}}$ (S. Laha et al. 2016; S. Mestici et al. 2024). Here we assume that volume filling factor is $V_{\rm f} \sim 1$ and that the number density of hydrogen $n_{\rm H}$ is roughly equal to electron $n_{\rm e}$ in the wind for simplification.

The ionizing luminosity $L_{\rm ion}$ is over the 13.6 eV–13.6 keV band. The mass outflow rate at $R_{\rm max}$ thus can be calculated with $\dot{M}_{\rm max} = 4\mu\pi m_{\rm p} L_{\rm ion} \xi^{-1} v_{\rm wind} C_{\rm f}$, where the average relative atomic mass $\mu \simeq 1.4$ and a covering factor $C_{\rm f} \sim 0.5$ is assumed (S. Mestici et al. 2024). We perform bootstrapping to determine the range of the 90% confidence level of the derived $R_{\rm max}$. We have also estimated the lower limit of the mass outflow rate $\dot{M}_{\rm min} = 8\mu\pi m_{\rm p} G M_{\rm BH} N_{\rm H} v_{\rm wind}^{-1} C_{\rm f}$ for UFO and WA, assuming the wind is launched where its velocity exceeds the local escape velocity. We have to emphasize that this estimation suffers from large uncertainties.

The bolometric luminosity of AGN implies the energy released by the accretion material at the event horizon of the central black hole. The mass inflow rate at the event horizon would be estimated by $\dot{M}_{\rm in} = \frac{L_{\rm bol}}{\epsilon c^2}$, where ϵ refers to the radiation efficiency. For radiatively inefficient hot accretion flows, ϵ decreases with the decreasing of the Eddington ratio $R_{\rm Edd} \equiv \frac{L_{\rm bol}}{L_{\rm Edd}}$ and falls below that of the standard thin disk ($\epsilon_{\rm SSD} \simeq 0.1$) in the low-luminosity regime. In this paper, we adopt the radiation efficiency ϵ from the theoretical ϵ-$\frac{\dot{M}_{\rm in}}{\dot{M}_{\rm Edd}}$ correlation provided in F.-G. Xie & F. Yuan (2012), assuming the fraction from viscous heating is $\delta \sim 0.5$. Their results are consistent with A. Sądowski & M. Gaspari (2017). The Eddington accretion rate is defined as $\dot{M}_{\rm Edd} \equiv 10 L_{\rm Edd}/c^2$. Therefore, the ratio between the net inflow rate at event horizon and the Eddington accretion rate is linked to the Eddington ratio $R_{\rm Edd} \equiv \frac{\epsilon \dot{M}_{\rm in}}{0.1 \dot{M}_{\rm Edd}}$, and thus given any Eddington ratio $R_{\rm edd}$ we would be able to precisely determine the net inflow rate at event horizon.

3. Results

We compare the putative truncation radii estimated from the wind velocity using the theory of wind in our sample as a function of the Eddington ratio, with the fiducial correlation taken from F. Yuan & R. Narayan (2014); the result is shown in the left panel of Figure 1. The fiducial truncation radii were determined by broadband spectral energy distribution (SED) fitting with RIAF models (F. Yuan & R. Narayan 2004). LLAGNs with UFO are roughly more consistent with the MAD98 case. M81* and NGC 7213, where HWs have been confirmed through highly ionized iron emission lines, together with Mrk 205 and NGC 4151 with UFOs generally follow the trend that $r_{\rm tr}$ increases as the accretion power decreases. This trend between $R_{\rm edd}$ and $r_{\rm tr}$ deduced from black hole wind is quantitatively consistent with the theoretical prediction from spectral modeling, while $r_{\rm tr}$ estimated from WA components is in general larger than the fiducial values.

The right panel of Figure 1 shows the comparison between $r_{\rm tr}$ and wind location $R_{\rm max}$ deduced from photoionization modeling. We can see from the figure that the estimated $r_{\rm tr}$ for both UFO and HW is in line with $R_{\rm max}$, especially in the case of MAD with high BH spin. In contrast, WAs lie above the line where $R_{\rm max} = r_{\rm tr}$. For UFO and HW, the detection location is close to the black hole and, more specifically, close to the truncation radius. Therefore, the detected wind velocity would be roughly consistent with the initial velocity of wind at its launching point. Our assumption is valid that the wind velocity originating from the truncation radius remains almost constant before encountering the ISM (C. Cui & F. Yuan 2020). However, for WA, the detection location seems far away from the wind launching region. One possible scenario is that although in LLAGNs outflows are driven mainly from $r_{\rm tr}$, the detected WAs trace the wind components located at a larger radius ($\gtrsim 10^5\, r_{\rm g}$) away from their origin points. Only at such large distances is the ionization state of WA lower and "suitable" to be detected in the soft X-rays. As the distance is further away, WAs may be opt to experience deceleration through interacting with the ISM, resulting in a larger putative truncation radius, according to Equations (2)–(5), with smaller wind velocity than expected. Since WAs may not trace the launching site of winds in the LLAGN, the intrinsic truncation radius of these AGN would be much smaller than deduced. Moreover, as the distance increases, the initially driven wind is expected to entrain more and more mass (M. Gaspari & A. Sądowski 2017), so the mass outflow rate estimation of these WAs would not reflect the intrinsic black hole wind.

Wind driven by hot accretion flow is expected to carry a substantial amount of material away. The radial profile of its mass outflow rate can be described by $\dot{M}_{\rm out,max} = \dot{M}_{\rm in}(\frac{r}{40\ r_{\rm g}})$ according to numerical simulations (F. Yuan et al. 2015). $\dot{M}_{\rm in}$ refers to the mass accretion rate at the event horizon (see Section 2.2). We investigate the ratio between the wind mass flux and black hole accretion rate (also known as the mass loading factor) for our sample. The results are shown in Figure 2. For UFO together with HW, the ratio is consistent with the theoretical estimation, while all the WAs are systematically offset from the expected correlation. F. Fiore et al. (2024) collect a sample of wind components mostly detected in AGN with an intermediate and high accretion rate and suggest a negative power-law correlation between the mass loading factor and the Eddington ratio. However, in our LLAGN wind sample, we do not find such a strong correlation, and the mass loading factors are on average larger than their high accretion rate counterparts. This adds further support to a different wind launching mechanism between hot-mode and cold-mode accretion.

4. Detailed Analysis on the Prototype M81*

Among all the selected samples, M81* is the closest archetypal LLAGN and has the most abundant multiwavelength observations over the past two decades. It is also one of the only two LLAGNs where evidence of HW has been confirmed by high-resolution X-ray spectroscopy. In this section, we take M81 as an example to compare the observational results and theoretical prediction of HW.

4.1. Truncation Radius

There are several ways to determine the truncation radius. By fitting the broadband SED of M81* with the ADAF + thin disk model, E. Quataert et al. (1999) found the truncation radius would be around $10^2\, r_{\rm g}$, and R. S. Nemmen et al. (2014) gave an updated estimation of $360\, r_{\rm g}$. The second way relates to the fluorescent 6.4 keV iron Kα line. Assuming it is generated from the Keplerian rotating cold outer thin disk illuminated by primary emission from the hot X-ray corona, from its line width $\sigma_{\rm v}$ we would determine $r_{\rm tr} \gtrsim 4.6 \times 10^2 - 1.9 \times 10^4\, r_{\rm g}$ for M81* (A. J. Young et al. 2007; F. Shi et al. 2021). The real $r_{\rm tr}$ could be even larger than the above estimation since A. J. Young et al. (2018) concludes that fluorescent Fe Kα line in M81* is produced from optically thin material within the $r_{\rm tr}$. The third way is from the reflection fraction $R_{\rm refl}$. The weak reflection component in the X-ray spectra of M81* indicates an lower limit of the truncation

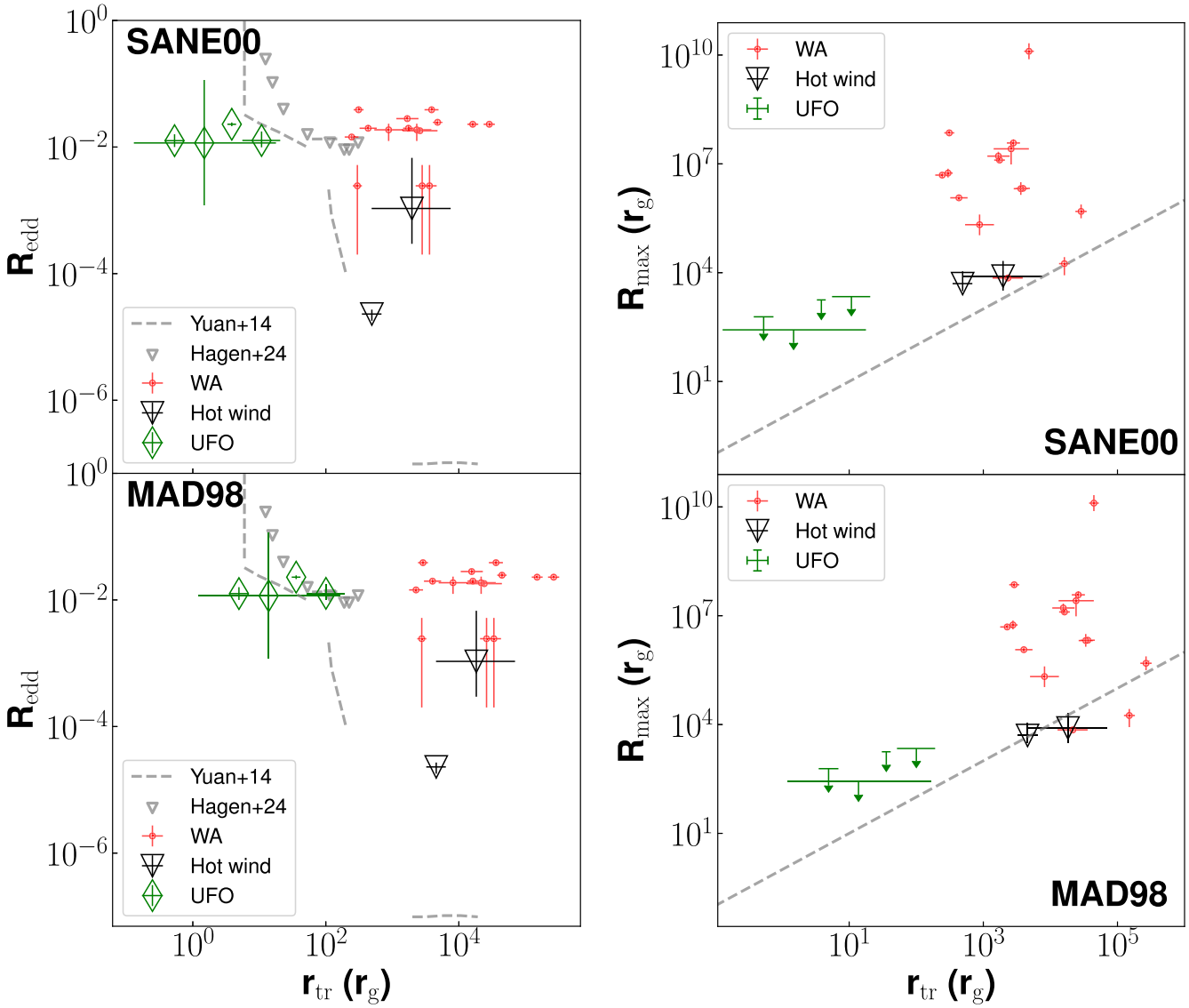

Figure 1. Left panel: putative truncation radius r_{tr} of the selected sample as a function of the Eddington ratio R_{Edd}, assuming driven by SANE00 (top panel) and MAD98 (bottom panel). Gray dashed lines and triangles present the fiducial value from the SED fitting given by previous studies for comparison, taken from F. Yuan & R. Narayan (2014) and S. Hagen et al. (2024), respectively. Green arrows denote the UFOs. Black triangles describe wind detected with highly ionized emission lines (HW). Red diamonds represent the WAs. The putative r_{tr} of UFO and HW in the MAD98 case is more consistent with the fiducial relation. Right panel: wind location R_{max} determined from spectral modeling compared with putative r_{tr} for SANE00 (top) and MAD98 (bottom). The gray dashed line marks where $r_{tr} = R_{max}$.

radius $r_{tr} \gtrsim (3-9) \times 10^2\, r_g$ (A. J. Young et al. 2018; F. Shi et al. 2021). The derived truncation radius of these various method is roughly consistent with that predicted by hot accretion flow theory (F. Yuan & R. Narayan 2004).

4.2. Velocity of Wind

As we have introduced in Section 2.1, the theory of wind (F. Yuan et al. 2012a, 2015) predicts that the wind speed should be proportional to the Keplerian speed at the wind launching radius (in this case, the truncation radius). Using the abovementioned observationally estimated truncation radius, this theory predicts that the velocity of wind would be $(0.46\text{–}3.1) \times 10^3\,\mathrm{km\,s^{-1}}$ for SANE00 and $(1.4\text{–}9.6) \times 10^3\,\mathrm{km\,s^{-1}}$ for MAD98. The observed wind velocity of M81* derived from X-ray spectroscopy is $\sim 2.8 \times 10^3\,\mathrm{km\,s^{-1}}$. This value is well within the predicted range.

Specifically, in the customized HW simulation for M81*, $r_{tr} = 3000\ r_g$ is adopted in F. Shi et al. (2021). The corresponding Keplerian velocity of this radius is $v_k \sim 5.4 \times 10^3\,\mathrm{km\,s^{-1}}$. Assuming in M81 the accretion flow is MAD and the black hole is rapidly spinning, the wind theory predicts a speed of $v_{wind} \sim 3.5 \times 10^3\,\mathrm{km\,s^{-1}}$. The observed wind velocity is well consistent with this prediction.

4.3. Mass Accretion Rate at the Event Horizon

The bolometric luminosity of M81* is $\sim 2.3 \times 10^{-5} L_{Edd}$. Using the result of radiative efficiency as a function of the mass accretion rate at the black hole horizon presented in F.-G. Xie & F. Yuan (2012; as described in Section 2.2), we can obtain the net accretion rate at the event horizon of the black hole $\dot{M}_{in}(r_{EH}) = \frac{L_{bol}}{\eta c^2} \sim 8.5 \times 10^{-5}\, M_\odot\ \mathrm{yr^{-1}}$.

4.4. Mass Flux of Wind

The theory of HW has predicted that most of the accretion material should be lost in wind and only a small fraction can

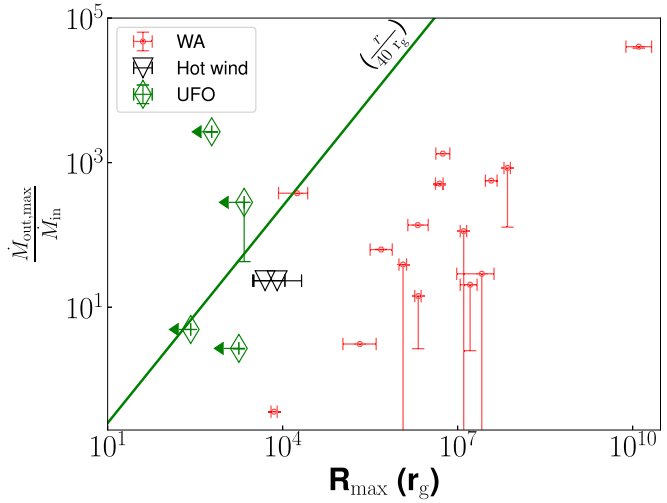

Figure 2. Ratio between the observationally derived mass flux of wind $\dot{M}_{\rm out,max}$ at $R_{\rm max}$ and the black hole accretion rate $\dot{M}_{\rm in} = \frac{L_{\rm bol}}{\epsilon c^2}$ as a function of wind location $R_{\rm max}$. The vertical solid line below each data point indicates the estimated lower limit of the mass flux $\dot{M}_{\rm out,max}$ for each detected wind component. The green solid line denotes the theoretical prediction for the mass flux of wind, $\frac{\dot{M}_{\rm out,max}}{\dot{M}_{\rm in}} = \frac{r}{40\ r_g}$ (F. Yuan et al. 2015). Other captions are similar to Figure 1.

finally reach the black hole. In other words, the mass flux of wind should be roughly equal to the mass flux at the outer boundary of the hot accretion flow, i.e., the truncation radius (F. Yuan et al. 2012a, 2012b, 2015). In this subsection, we use observational data of M81 to examine this prediction.

A. Schnorr Müller et al. (2011) estimated a mass inflow rate of $\dot{M}_{\rm in}(17\ {\rm pc}) \sim 4 \times 10^{-3}\ M_\odot\ {\rm yr}^{-1}$ from the observed kinematics of ionized gas within ~17 pc ($5 \times 10^6 r_g$). Since this location is much larger than the estimated truncation radius above, this ionized gas should supply the outer accretion thin disk. Wind exists in the thin disk, and the mass flux of wind is about half of the inflow rate in the disk (see Figure 7 in W. Wang et al. 2022). Thus, the mass inflow rate left at the innermost radius of the thin disk, i.e., the truncation radius, would be $\dot{M}_{\rm in,net}(r_{\rm tr}) \sim 0.5\dot{M}_{\rm in}(17{\rm pc}) \sim 2 \times 10^{-3}\ M_\odot\ {\rm yr}^{-1}$.

By comparing the observed highly ionized iron emission lines with the HW modeling from customized numerical simulations, F. Shi et al. (2021) reported a mass outflow rate $\dot{M}_{\rm out} \sim 2 \times 10^{-3}\ M_\odot\ {\rm yr}^{-1}$ of HW in M81*. This is in excellent agreement with the prediction of theory of wind.

4.5. Radial Profile of Hot Accretion Inflow

Combining the mass accretion rates at the black hole event horizon and at the truncation radius obtained in the previous two subsections, we can estimate the index s of the radial profile of accretion rate $\dot{M}_{\rm in,net}(r_{\rm s}) = \dot{M}_{\rm in}(r_{\rm tr})\left(\frac{r_{\rm EH}}{r_{\rm tr}}\right)^s$ (e.g., F. Yuan et al. 2012b). It is found to be $s \sim 0.43$ using $r_{\rm tr} = 3000 r_g \equiv 1500\ r_{\rm s}$ in M81*. This is well consistent with the theoretical prediction (F. Yuan et al. 2012b; H. Yang et al. 2021). Specifically, H. Yang et al. (2021) predict the index s to be 0.42 for the case of MAD and black hole spin $a = 0.98$, which matches with the obtained s in M81* quite well.

The above result suggests that the accretion flow in M81 is MAD, and the black hole should be rapidly spinning. This is consistent with the fact that a jet exists in M81, assuming the jet formation theory proposed by R. D. Blandford & R. L. Znajek (1977). We note that this theory of jet formation recently has obtained new strong observational evidence. H. Yang et al. (2024) have performed a GRMHD numerical simulation of black hole accretion and jet formation. Assuming that magnetic reconnection in the jet can efficiently accelerate electrons, with detailed calculation of electron acceleration and radiative transfer in the jet, they obtained the jet morphology, including the elongated structure, the limb-brightening feature, and the jet width as a function of distance to the black hole. Comparing these features with observations of the jet in M87, they find that the Blandford-Znajek (BZ) jet can nicely reproduce all these observed features, while other jet models, such as Blandford–Payne (BP) model, cannot. Moreover, the mode of the accretion flow should be MAD rather than SANE, and the black hole spin should be large. Our current results strongly suggest that, like M87, the accretion flow in M81* should also be MAD, and the black hole spin in M81 should also be large.

4.6. Jet-to-wind Power Ratio

In the case of M81*, the kinetic power of HW is estimated to be $\sim 2 \times 10^{40}\ {\rm erg\ s}^{-1}$ (F. Shi et al. 2021). Radio emission from M81* is highly variable, with an average 1.4 GHz flux density of 0.09–0.62 Jy (R. L. White & R. H. Becker 1992; J. J. Condon et al. 1998). Based on the empirical relation of jet mechanical power $L_{\rm mech} = 7 \times 10^{36} f (L_{1.4\ {\rm GHz}}/10^{25}\ {\rm W\ Hz}^{-1})^{0.68}{\rm W}$ and assuming the calibration factor $f = 4$ (T. M. Heckman & P. N. Best 2014), we roughly estimate the mechanical power of the jet in M81* would be around $(1.39 - 5.22) \times 10^{41}\ {\rm erg\ s}^{-1}$. The kinetic power carried by jet is around several times that carried by the HW in M81*. This is consistent with the prediction for an MAD around an extremely spinning black hole, where the ratio of kinetic energy between the jet and HW would be ~4 (H. Yang et al. 2021).

In summary, we find good agreement between the theory of wind launched from a hot accretion flow and observations, including the speed and mass flux of the wind, the power-law index of the radial profile of inflow rate, and the jet-to-wind power ratio.

5. Summary and Discussion

In this paper, we collect a sample of outflows (including HW, UFOs, and WAs) detected in low-luminosity AGN ($R_{\rm Edd} \lesssim 0.04$). The inner accretion disk of these supermassive black holes (SMBHs) with low accretion rates could be truncated and replaced by radiatively inefficient hot accretion flow. We compare the theoretical predictions of wind driven by such hot accretion flow with observed wind properties. Furthermore we analyze the multiple kinetic properties of inflow and outflow detected in M81* reported by multiwavelength observations. We take this closest prototypical LLAGN as a test case for the state-of-art theory of wind launched from hot accretion flows. Our main results are as follows:

1. We have compared the truncation radii obtained from wind velocity based on the theory of wind in our sample with the values of truncation radius obtained from other constraints. Good consistency is found, providing strong support to the theory of wind.
2. We investigate the ratio between the wind mass flux and black hole accretion rate for our sample. For UFO together with HW, the ratio is consistent with the theoretical prediction.

3. For M81, using the truncation radius $r_{\rm tr} = 3000\, r_g$ obtained from broadband fitting, reflection fraction, and Fe Kα lines, the theory of wind predicts a speed of $\sim 3.5 \times 10^3\,{\rm km\,s^{-1}}$, very similar to the observed value of $\sim 2.8 \times 10^3\,{\rm km\,s^{-1}}$.
4. The spectroscopy deduced outflow rate of the HW in M81* is roughly equal to the net inflow rate of warm ionized gas, which should be the inflow rate at the truncation radius. This is consistent with the theoretical expectation.
5. The observed inflow rates at event horizon $r_{\rm EH}$ and at truncation radius $r_{\rm tr}$ suggest that the value of power index in the radial profile $\dot{M}_{\rm in,net}(r_{\rm s}) = \dot{M}_{\rm in}(r_{\rm tr})\left(\frac{r_{\rm EH}}{r_{\rm tr}}\right)^s s \sim 0.43$. This is consistent with the predicted value of $s \sim 0.42$ for the case of MAD-type hot accretion flow around an extremely spinning black hole.

We must emphasize that the wind velocity derived from observations may be subject to the projection effect of the viewing angle and wind properties derived from photoionization modeling, such as ξ, $N_{\rm H}$, and $R_{\rm max}$, have large uncertainties. More attention should be paid to the outflows in the low-luminosity end of AGNs to achieve a larger and more accurate sample with the help of the new generation of X-ray telescopes like XRISM.

Acknowledgments

We would like to thank Suoqing Ji and Defu Bu for helpful discussions. F.S. is supported in part by the China Postdoctoral Science Foundation (grants 2022TQ0354 and 2022M723279). F.Y. is supported by Natural Science Foundation of China (grants 12133008, 12192220, 12192223, and 12361161601) and the China Manned Space Project (CMS-CSST-2021-B02).

ORCID iDs

Fangzheng Shi (施方正) https://orcid.org/0000-0003-3922-5007
Feng Yuan https://orcid.org/0000-0003-3564-6437
Francesco Tombesi https://orcid.org/0000-0002-6562-8654
Fu-guo Xie https://orcid.org/0000-0001-9969-2091

References

Abramowicz, M. A., Czerny, B., Lasota, J. P., & Szuszkiewicz, E. 1988, ApJ, 332, 646
Andrade-Velázquez, M., Krongold, Y., Elvis, M., et al. 2010, ApJ, 711, 888
Bentz, M. C., & Katz, S. 2015, PASP, 127, 67
Blandford, R. D., & Begelman, M. C. 1999, MNRAS, 303, L1
Blandford, R. D., & Znajek, R. L. 1977, MNRAS, 179, 433
Bu, D.-F., Yuan, F., Gan, Z.-M., & Yang, X.-H. 2016, ApJ, 818, 83
Cheung, E., Bundy, K., Cappellari, M., et al. 2016, Natur, 533, 504
Condon, J. J., Cotton, W. D., Greisen, E. W., et al. 1998, AJ, 115, 1693
Crenshaw, D. M., & Kraemer, S. B. 2012, ApJ, 753, 75
Cui, C., & Yuan, F. 2020, ApJ, 890, 81
Esin, A. A., McClintock, J. E., & Narayan, R. 1997, ApJ, 489, 865
Fabian, A. C. 2012, ARA&A, 50, 455
Fiore, F., Feruglio, C., Shankar, F., et al. 2017, A&A, 601, A143
Fiore, F., Gaspari, M., Luminari, A., Tozzi, P., & de Arcangelis, L. 2024, A&A, 686, A36
Fukumura, K., Dadina, M., Matzeu, G., et al. 2022, ApJ, 940, 6
Gaspari, M., & Sądowski, A. 2017, ApJ, 837, 149
Hagen, S., Done, C., Silverman, J. D., et al. 2024, MNRAS, 534, 2803
Heckman, T. M., & Best, P. N. 2014, ARA&A, 52, 589
Ho, L. C. 2008, ARA&A, 46, 475
Kormendy, J., & Ho, L. C. 2013, ARA&A, 51, 511
Kraemer, S. B., George, I. M., Crenshaw, D. M., et al. 2005, ApJ, 633, 693
Laha, S., Guainazzi, M., Chakravorty, S., Dewangan, G. C., & Kembhavi, A. K. 2016, MNRAS, 457, 3896
Laha, S., Guainazzi, M., Dewangan, G. C., Chakravorty, S., & Kembhavi, A. K. 2014, MNRAS, 441, 2613
Markowitz, A., Reeves, J. N., George, I. M., et al. 2009, ApJ, 691, 922
Matzeu, G. A., Brusa, M., Lanzuisi, G., et al. 2023, A&A, 670, A182
McKernan, B., Yaqoob, T., & Reynolds, C. S. 2007, MNRAS, 379, 1359
Mehdipour, M., & Costantini, E. 2019, A&A, 625, A25
Mehdipour, M., Kriss, G. A., Kaastra, J. S., et al. 2021, A&A, 652, A150
Mestici, S., Tombesi, F., Gaspari, M., Piconcelli, E., & Panessa, F. 2024, MNRAS, 532, 3036
Narayan, R., SÄ dowski, A., Penna, R. F., & Kulkarni, A. K. 2012, MNRAS, 426, 3241
Narayan, R., & Yi, I. 1994, ApJL, 428, L13
Narayan, R., & Yi, I. 1995, ApJ, 452, 710
Nemmen, R. S., Storchi-Bergmann, T., & Eracleous, M. 2014, MNRAS, 438, 2804
Quataert, E., Di Matteo, T., Narayan, R., & Ho, L. C. 1999, ApJL, 525, L89
Reynolds, C. S., Lohfink, A. M., Ogle, P. M., et al. 2015, ApJ, 808, 154
Schnorr Müller, A., Storchi-Bergmann, T., Riffel, R. A., et al. 2011, MNRAS, 413, 149
Shakura, N. I., & Sunyaev, R. A. 1973, A&A, 24, 337
Shi, F., Li, Z., Yuan, F., & Zhu, B. 2021, NatAs, 5, 928
Shi, F., Yuan, F., Li, Z., Su, Z., & Ji, S. 2024, ApJ, 970, 48
Shi, F., Zhu, B., Li, Z., & Yuan, F. 2022, ApJ, 926, 209
Sądowski, A., & Gaspari, M. 2017, MNRAS, 468, 1398
Steenbrugge, K. C., Kaastra, J. S., Crenshaw, D. M., et al. 2005, A&A, 434, 569
Storchi-Bergmann, T., Eracleous, M., Teresa Ruiz, M., et al. 1997, ApJ, 489, 87
Tombesi, F., Cappi, M., Reeves, J. N., et al. 2010, A&A, 521, A57
Tombesi, F., Cappi, M., Reeves, J. N., et al. 2011, ApJ, 742, 44
Tombesi, F., Cappi, M., Reeves, J. N., et al. 2013, MNRAS, 430, 1102
Wang, Q. D., Nowak, M. A., Markoff, S. B., et al. 2013, Sci, 341, 981
Wang, W., Bu, D.-F., & Yuan, F. 2022, MNRAS, 513, 5818
Wang, Y., Kaastra, J., Mehdipour, M., et al. 2022, A&A, 657, A77
Weinberger, R., Springel, V., Hernquist, L., et al. 2017, MNRAS, 465, 3291
White, R. L., & Becker, R. H. 1992, ApJS, 79, 331
Xie, F.-G., & Yuan, F. 2012, MNRAS, 427, 1580
Yang, H., Yuan, F., Li, H., et al. 2024, SciA, 10, eadn3544
Yang, H., Yuan, F., Yuan, Y.-F., & White, C. J. 2021, ApJ, 914, 131
Yoon, D., Yuan, F., Ostriker, J. P., Ciotti, L., & Zhu, B. 2019, ApJ, 885, 16
Young, A. J., McHardy, I., Emmanoulopoulos, D., & Connolly, S. 2018, MNRAS, 476, 5698
Young, A. J., Nowak, M. A., Markoff, S., Marshall, H. L., & Canizares, C. R. 2007, ApJ, 669, 830
Yuan, F., Bu, D., & Wu, M. 2012a, ApJ, 761, 130
Yuan, F., Gan, Z., Narayan, R., et al. 2015, ApJ, 804, 101
Yuan, F., & Narayan, R. 2004, ApJ, 612, 724
Yuan, F., & Narayan, R. 2014, ARA&A, 52, 529
Yuan, F., Wu, M., & Bu, D. 2012b, ApJ, 761, 129
Yuan, F., Yoon, D., Li, Y.-P., et al. 2018, ApJ, 857, 121